Organometallic Reactivity on a Calix[4]arene Oxo Surface. The Stepwise Migratory Insertion of Carbon Monoxide and Isocyanides into Zirconium−Carbon Bonds Anchored to a Calix[4]arene Moiety

Luca Giannini,[†] Alessandro Caselli,[†] Euro Solari,[†] Carlo Floriani,*[,†] Angiola Chiesi-Villa,[‡] Corrado Rizzoli,[‡] Nazzareno Re,[§] and Antonio Sgamellotti[§]

Contribution from the Institut de Chimie Minérale et Analytique, BCH, Université de Lausanne, CH-1015 Lausanne, Switzerland, Dipartimento di Chimica, Università di Parma, I-43100 Parma, Italy, and Dipartimento di Chimica, Università di Perugia, I-06100 Perugia, Italy

Received March 13, 1997[⊗]

Abstract: The present report deals with the multistep migratory insertion of carbon monoxide and isocyanides into the metal−carbon bonds of the ZrR_2 fragment anchored to a tetroxo matrix, defined by the dimethoxycalix[4]arene dianion [*p*-Bu^t-calix[4]-$(OMe)_2(O)_2]^{2-}$. The relevant differences between the two fragments [*p*-Bu^t-calix[4]-$(OMe)_2(O)_2Zr]^{2+}$ and $[Cp_2Zr]^{2+}$ are experimentally proven and theoretically interpreted. Unlike those for $[Cp_2Zr]^{2+}$ derivatives, the reaction of CO with [*p*-Bu^t-calix[4]-$(OMe)_2(O)_2ZrR_2$] [R = Me, **1**; CH_2Ph, **2**; *p*-MeC_6H_4, **3**] proceeds *via* a two-step migration directly to the corresponding η^2-metal-bonded-ketones [*p*-Bu^t-calix[4]-$(OMe)_2(O)_2Zr\{\eta^2$-$C(R_2)O]$ (R = Me, **4**; CH_2Ph, **5**; *p*-MeC_6H_4, **6**). The Zr−C functionality in **4**−**6** maintains its inserting capability in the reaction with ketones, *i.e.*, Ph_2CO, leading to the diolate derivative [*p*-Bu^t-calix[4]-$(OMe)_2(O)_2Zr\{OC(R_2)C(Ph_2)O\}$] (**8**, R = *p*-$MeC_6H_4$), or with Bu^{t}NC, forming [*p*-Bu^t-calix[4]-$(OMe)_2(O)_2Zr\{OC(Me_2)C(CNBu^t)N(Bu^t)\}$] (**7**). The reaction of **1**−**3** with Bu^{t}NC proceeds through two different pathways, depending on the temperature and the R substituent at the metal. The first one leads to the η^2-metal-bonded imine [*p*-Bu^t-calix[4]-$(OMe)_2(O)_2Zr\{\eta^2$-$N(Bu^t)C(R_2)\}$] [R = Me, **12**; CH_2Ph, **13**], which inserts two additional molecules of Bu^{t}NC to give a metalladiazacyclopentane, [*p*-Bu^t-calix[4]-$(OMe)_2(O)_2Zr\{N(Bu^t)C(Me_2)C(CNBu^t)N(Bu^t)\}$] (**14**). The second pathway led, at low temperature, to the bis-η^2-iminoacyls [*p*-Bu^t-calix[4]-$(OMe)_2(O)_2Zr\{\eta^2$-$N(Bu^t)=C(R)\}_2$] [R = Me, **15**; *p*-MeC_6H_4, **16**], which at 60 °C couple to the corresponding enediamido ligand in [*p*-Bu^t-calix[4]-$(OMe)_2(O)_2Zr$-$\{N(Bu^t)C(R)=C(R)N(Bu^t)\}$] [R = Me, **17**; *p*-$MeC_6H_4$, **18**]. The coupling of **15** and **16** showed first order kinetics in both cases and allowed the calculation of the corresponding activation parameters. The most significant differences between [*p*-Bu^t-calix[4]-$(OMe)_2(O)_2Zr]^{2+}$ and $[Cp_2Zr]^{2+}$ have been interpreted on the basis of the frontier orbital sets of the two fragments.

Introduction

Calix[4]arenes exemplify,[1] at the molecular level, the chemical environment that an organometallic fragment is supposed to experience when anchored to solid state supports, such as oxides or zeolites.[2] Although the anchoring groups in calix[*n*]arene are methylene-bridged phenoxo anions, the role of calix[*n*]arene as an ancillary ligand is different from that played by the same number of monomeric phenoxo moieties. This is easily understood for the following reasons: (i) the calix[4]arene provides a nearly planar oxo surface for anchoring the metal; (ii) the charge provided by the O_4 moiety can be adjusted from −4 to −2 *via* partial methylation of the phenoxo groups, thus creating the possibility of having functionalizable sites at the metal. An additional advantage is the potential of using the calix[4]arene bridging methylene and the Bu^t groups as spectroscopic probes for revealing the symmetry of the fragment attached to the transition metal.

In order to emphasize the peculiar role of calix[4]arene as a supporting ligand[3−5] compared to cyclopentadienyl and phenoxo anions, we chose the Zr−C bond for its versatility and potential in organic synthesis[6,7] and focused on one of the most useful, and as it turned out peculiar, reactions, namely the migratory insertion of carbon monoxide and isocyanides.[8] Herein, we report the kinetically and structurally defined stepwise

* To whom correspondence should be addressed.
[†] Université de Lausanne.
[‡] Università di Parma.
[§] Università di Perugia.
[⊗] Abstract published in *Advance ACS Abstracts,* September 15, 1997.

(1) Gutsche, C. D. *Calixarenes*; The Royal Society of Chemistry: Cambridge, U.K., 1989. (b) *Calixarenes, A Versatile Class of Macrocyclic Compounds*; Vicens, J., Böhmer, V., Eds.; Kluwer: Dordrecht, The Netherlands, 1991.

(2) (a) Corker, J.; Lefebvre, F.; Lecuyer, C.; Dufaud, V.; Quignard, F.; Choplin, A.; Evans, J.; Basset, J.-M. *Science* **1996**, *271*, 966−969. (b) Niccolai, G. P.; Basset, J.-M. *Appl. Catal. A* **1996**, *146*, 145−156. (c) Vidal, V.; Theolier, A.; Thivolle-Cazat, J.; Basset, J.-M.; Corker, J. *J. Am. Chem. Soc.* **1996**, *118*, 4595−4662.

(3) Giannini, L.; Solari, E.; Zanotti-Gerosa, A.; Floriani, C.; Chiesi-Villa, A.; Rizzoli, C. *Angew. Chem., Int. Ed. Engl.* **1996**, *35*, 85−87.

(4) Castellano, B.; Zanotti-Gerosa, A.; Solari, E.; Floriani, C.; Chiesi-Villa, A.; Rizzoli, C. *Organometallics* **1996**, *15*, 4894−4896.

(5) (a) Giannini, L.; Solari, E.; Zanotti-Gerosa, A.; Floriani, C.; Chiesi-Villa, A.; Rizzoli, C. *Angew. Chem., Int. Ed. Engl.* **1996**, *35*, 2825−2827. (b) Giannini, L.; Solari, E.; Zanotti-Gerosa, A.; Floriani, C.; Chiesi-Villa, A.; Rizzoli, C. *Angew. Chem., Int. Ed. Engl.* In press. (c) Gardiner, M. G.; Lawrence, S. M.; Raston, C. L.; Skelton, B. W.; White, A. H. *Chem. Commun.* **1996**, 2491. (d) Gardiner, M. G.; Koutsantonis, G. A.; Lawrence, S. M.; Nichols, P. J.; Raston, C. L. *Chem. Commun.* **1996**, 2035. (e) Gibson, V. C.; Redshaw, C.; Clegg, W.; Elsegood, M. R. J. *J. Chem. Soc., Chem. Commun.* **1995**, 2371. (f) Acho, J. A.; Doerrer, L. H.; Lippard, S. J. *Inorg. Chem.* **1995**, *34*, 2542.

S0002-7863(97)00822-6 CCC: $14.00

insertion processes occurring on the dialkyl derivatives shown below:

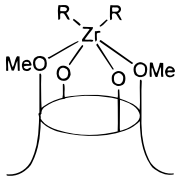

[*p*-Bu^t-calix[4]-(OMe)$_2$(O)$_2$ZrR$_2$]

These reactions proceed *via* metal-assisted C−C bond formation and lead to a variety of carbon−metal-bonded fragments supported by the unusual tetraoxo [calix[4]-(OMe)$_2$(O)$_2$]$^{2-}$ dianion in a quasi-planar arrangement. A preliminary report on this subject appeared recently.[3] Extended Hückel calculations have been performed with the purpose of rationalizing the major differences between the [Cp$_2$Zr]$^{2+}$ and the [calix[4]-(OMe)$_2$(O)$_2$Zr]$^{2+}$ fragments in driving migratory insertion reactions.

Experimental Section

All operations were carried out under an atmosphere of purified nitrogen. All solvents were purified by standard methods and freshly distilled prior to use. NMR spectra were recorded on 200-AC and 400-DPX Bruker instruments. The syntheses of **1**−**3** are described in detail elsewhere.[9] The content of solvent of crystallization has been checked by thermal treatment of the sample followed by a gas chromatography analysis.

Synthesis of 4. Complex **1**·C$_6$H$_6$ (5.29 g, 6.06 mmol) was suspended in benzene (150 mL), and the N$_2$ was replaced with CO at room temperature. The mixture became colorless in a few minutes. After 1 h, volatiles were removed *in vacuo* and hexane (50 mL) was added to the residue. The flask was kept at −25 °C for 14 h, and then the white **4** was collected at −20 °C and dried *in vacuo* (4.18 g, 83.7%). ^{1}H NMR (C$_6$D$_6$, 298 K): δ = 7.25 (d, J = 2.5 Hz, 2H, ArH), 7.21 (d, J = 2.5 Hz, 2H, ArH), 6.89 (s, 2H, ArH), 6.81 (s, 2H, ArH), 4.45 (d, J = 12.5 Hz, 2H, *endo*-CH$_2$), overlapping with 4.43 (s, 3H, MeO), overlapping with 4.42 (d, J = 12.5 Hz, 2H, *endo*-CH$_2$), 4.20 (s, 3H, MeO), 3.27 (d, J = 12.5 Hz, 2H, *exo*-CH$_2$), 3.15 (d, J = 12.5 Hz, 2H, *exo*-CH$_2$), 2.11 (s, 6H, Me), 1.45 (s, 18H, Bu^t), 0.77 (s, 9H, Bu^t), overlapping with 0.74 (s, 9H, Bu^t). ^{1}H NMR (CD$_2$Cl$_2$, 298 K): δ 7.14 (d, J = 2.5 Hz, 2H, ArH), 7.12 (d, J = 2.5 Hz, 2H, ArH), 7.08 (s, 2H, ArH), 7.04 (s, 2H, ArH), 4.66 (s, 3H, MeO), 4.62 (s, 3H, MeO), 4.41 (d, J = 12.4 Hz, 2H, *endo*-CH$_2$), 4.35 (d, J = 12.4 Hz, 2H, *endo*-CH$_2$), 3.41 (d, J = 12.4 Hz, 2H, *exo*-CH$_2$), 3.35 (d, J = 12.4 Hz, 2H, *exo*-CH$_2$), 1.68 (s, 6H, Me), 1.27 (s,18H, Bu^t), 1.11 (s, 9H, Bu^t), overlapping with 1.13 (s, 9H, Bu^t). Anal. Calcd for **4**, C$_{49}$H$_{64}$O$_5$Zr: C, 71.40; H, 7.83. Found: C, 71.15; H, 8.16. The product is thermally stable in C$_6$D$_6$ (14 h, 65 °C) but slowly decomposes when exposed to solar light.

Synthesis of 5. Compound **2** (5.56 g, 5.86 mmol) was dissolved in benzene (200 mL), and the N$_2$ atmosphere was replaced with CO. The mixture was stirred at room temperature for 30 min and became colorless. Volatiles were then removed *in vacuo*, and hexane (50 mL) was added to the residue. The flask was kept at −25 °C for 14 h, and the white **5**·(C$_6$H$_6$)$_{1.5}$ was collected and dried *in vacuo* (4.2 g, 65.5%). ^{1}H NMR (C$_6$D$_6$, 298 K): δ 7.63 (m, 4H, ArH(PhCH$_2$)), 7.24−7.15 (m, ArH), 6.90 (m, 2H, ArH(PhCH$_2$)), 6.82 (s, 2H, ArH), 6.79 (s, 2H, ArH), 4.45 (s, 3H, MeO), 4.22 (d, J = 12.4 Hz, 4H, *endo*-CH$_2$), 4.03 (s, 3H, MeO), 3.65 (d, J = 13 Hz, 2H, PhC*H*$_2$), 3.47 (d, J = 13 Hz, 2H, PhC*H*$_2$), 3.19 (d, J = 12.4 Hz, 2H, *exo*-CH$_2$), overlapping with 3.18 (d, J = 12.4 Hz, 2H, *exo*-CH$_2$), 1.44 (s, 18H, Bu^t), 0.74 (s, 9H, Bu^t), overlapping with 0.72 (s, 9H, Bu^t). ^{1}H NMR (CD$_2$Cl$_2$, 298 K): δ 7.51 (m, 4H, ArH(PhCH$_2$)), 7.40 (s, 9H, C$_6$H$_6$), 7.20 (m, 4H, ArH-(PhCH$_2$)), 7.05 (s, 4H, ArH), 6.98 (s, 4H, ArH), 6.88 (m, 2H, ArH-(PhCH$_2$)), 4.70 (s, 3H, MeO), 4.36 (s, 3H, MeO), 4.15 (d, J = 12.4 Hz, 2H, *endo*-CH$_2$), overlapping with 4.13 (d, J = 12.4 Hz, 2H, *endo*-CH$_2$), 3.31 (s, 4H, PhC*H*$_2$), 3.28 (d, J = 12.4 Hz, 2H, *exo*-CH$_2$), 3.22 (d, J = 12.4 Hz, 2H, *exo*-CH$_2$), 1.27 (s,18H, Bu^t), 1.11 (s, 9H, Bu^t), overlapping with 1.10 (s, 9H, Bu^t). Anal. Calcd for **5**·(C$_6$H$_6$)$_{1.5}$, C$_{70}$H$_{81}$O$_5$Zr: C, 76.88; H, 7.47. Found: C, 76.86; H, 7.66. Crystals suitable for X-ray analysis were obtained by cooling a saturated solution of **5** in hexane/benzene (*ca.* 7:1) to −25 °C. The product is thermally stable in C$_6$D$_6$ (14 h, 65 °C) but slowly decomposes when exposed to solar light. When a proton source is present, [*p*-Bu^t-calix[4]-(OMe)$_2$-(O)$_2$Zr{OCH(CH$_2$Ph)$_2$}$_2$] is easily formed.

Synthesis of 6. An ampule containing **3** (0.955 g, 1.01 mmol) was suspended in toluene (160 mL). The flask was saturated with CO. At 15 °C and at a pressure of 1.002 atm, the ampule was broken; 24.7 mL (1.04 mmol) of CO were absorbed during the reaction (complete in 5 min). The glass was filtered off, and the volatiles were removed *in vacuo*. *n*-Hexane was added to the residue, and the resulting solution was kept at −24 °C overnight. Compound **6** precipitated as a light yellow powder, which was collected and dried *in vacuo* (0.44 g, 45%). ^{1}H NMR (C$_6$D$_6$, 298 K): δ = 7.96 (d, J = 8.2 Hz, 4H, ArH), 7.18 (d, 4H, ArH), overlapping with 7.15 (s, 4H, ArH), 6.79 (s, 4H, ArH), 4.47 (s, 3H, MeO), overlapping with 4.43 (d, 4H, *endo*-CH$_2$), 4.32 (s, 3H, MeO), 3.15 (d, J = 12.4 Hz, 4H, *exo*-CH$_2$), 2.17 (s, 6H, CH$_3$), 1.39 (s, 18H, Bu^t), 0.75 (s, 9H, Bu^t), 0.68 (s, 9H, Bu^t). Anal. Calcd for **6**, C$_{61}$H$_{72}$O$_5$Zr: C, 75.03; H, 7.43. Found: C, 74.99; H, 7.78.

Synthesis of 7. Bu^{t}NC (0.61 g, 7.34 mmol) was added at room temperature to a solution of **4** (2.95 g, 3.57 mmol) in toluene (100 mL), and the resulting yellow solution was stirred for 7 h. Volatiles were removed *in vacuo* until near dryness, and hexane (40 mL) was added to the residue. The flask was kept for 2 days at −24 °C; the pale yellow **7**·C$_7$H$_8$·(C$_6$H$_{14}$)$_{0.5}$ was then collected and dried *in vacuo* (1.2 g, 30%). ^{1}H NMR (CD$_2$Cl$_2$, 298 K): δ = 7.35−7.0 (m, 13H, ArH, C$_7$H$_8$), 4.46 (s, 6H, MeO), 4.37 (d, J = 12.4 Hz, 1H, CH$_2$), overlapping with 4.34 (d, J = 12.4 Hz, 1H, CH$_2$), 4.25 (d, J = 12.8 Hz, 1H, CH$_2$), overlapping with 4.23 (d, J = 12.8 Hz, 1H, CH$_2$), 3.42−3.3 (m, 4H, CH$_2$), 2.38 (s, 3H, C$_7$H$_8$), 1.56 (s, 3H, Me), 1.54 (s, 9H, Bu^t), 1.46 (s, 3H, Me), 1.32 (s, 9H, Bu^t), overlapping with 1.31 (s, 13H, Bu^t), 1.29 (s, 9H, Bu^t), 1.18 (s, 18H, Bu^t), 0.93 (m, 3H, hexane). IR: (Nujol mull) 1973, 1952 cm^{-1} (s); (toluene solution) 1958 cm^{-1} (s). Anal. Calcd for **7**·C$_7$H$_8$·(C$_6$H$_{14}$)$_{0.5}$, C$_{69}$H$_{97}$O$_5$N$_2$Zr: C, 73.62; H, 8.68; N, 2.49. Found: C, 73.37; H, 8.83; N, 2.30.

Synthesis of 8. Compound **3** (5.46 g, 5.76 mmol) was dissolved in benzene (150 mL), and the N$_2$ atmosphere was replaced with CO. The mixture was stirred overnight in the dark to give a light yellow solution. CO was then replaced with N$_2$, and a solution of Ph$_2$CO (1.04 g, 5.70 mmol) in benzene (150 mL) added dropwise at room temperature, under stirring, to the reaction mixture. Volatiles were removed *in vacuo*, *n*-hexane was added to the residue, and the resulting solution was kept at −24 °C overnight. It was then frozen (liquid N$_2$) and allowed to warm to room temperature. After 4 h, **8**·(C$_6$H$_{14}$)$_{0.5}$·(C$_6$H$_6$)$_{0.5}$ precipitated as a white powder, which was collected and dried *in vacuo* (4.11 g, 58%). ^{1}H NMR (CD$_2$Cl$_2$, 298 K): δ 7.64 (m, 4H, ArH), 7.43 (d, J = 9.1 Hz, 4H, ArH), 7.36 (s, 3H, benzene), 7.17 (m, 6H, ArH), 7.09 (s,

(6) (a) Negishi, E.-I.; Takahashi, T. *Acc. Chem. Res.* **1994**, *27*, 124−130 and references therein. (b) Erker, G.; Pfaff, R. *Organometallics* **1993**, *12*, 1921−1926. (c) Reetz, M. T. In *Organometallics in Synthesis*; Schlosser, M., Ed.; Wiley: New York, 1994; Chapter 3. (d) Negishi, E.-I. In *Comprehensive Organic Synthesis*; Paquette, L. A., Ed.; Pergamon: Oxford, 1991; Vol. 5, p 1163. (e) Schore, N. E. In *Comprehensive Organic Synthesis*; Paquette, L. A., Ed.; Pergamon: Oxford, 1991; Vol. 5, p 1037. (f) Buchwald, S. L.; Nielsen, R. B. *Chem. Rev.* **1988**, *88*, 1047−1058. (g) Cardin, D. J.; Lappert, M. F.; Raston, C. L. *Chemistry of Organozirconium and Hafnium Compounds*; Wiley: New York, 1986.

(7) Coates, G. W.; Waymouth, R. M. In *Comprehensive Organometallic Chemistry II*; Abel, E. W., Stone, F. G. A., Wilkinson, G., Eds.; Pergamon: Oxford, 1995; Vol. 12, Chapter 12.1. Ryan, E. J. In *Comprehensive Organometallic Chemistry II*; Abel, E. W., Stone, F. G. A., Wilkinson, G., Eds.; Pergamon: Oxford, 1995; Vol. 4, Chapter 9. Jordan, R. F.; Lapointe, R. E.; Bradley, P. K.; Baenzinger, N. *Organometallics* **1989**, *8*, 2892 and references therein. Buchwald, S. L.; La Maire, S. J.; Nielsen, R. B.; Watson, B. T.; King, S. M. *Tetrahedron Lett.* **1987**, *28*, 3895. Neghishi, E.; Takahashi, T. *Aldrichim. Acta* **1985**, *18*, 31. Neghishi, E.; Miller, J. A.; Yoshida, T. *Tetrahedron Lett.* **1984**, *25*, 3407. Neghishi, E.; Yoshida, T. *Tetrahedron Lett.* **1980**, *21*, 1501. Schwartz, J. *Pure Appl. Chem.* **1980**, *52*, 733. Carr, D. B.; Yoshifuji, M.; Shoer, L. I.; Gell, K. I.; Schwartz, J. *Ann. N.Y. Acad. Sci.* **1977**, *295*, 127. Schwartz, J.; Labinger, J. A. *Angew. Chem., Int. Ed. Engl.* **1976**, *15*, 333.

(8) Durfee, L. D.; Rothwell, I. P. *Chem. Rev.* **1988**, *88*, 1059−1079 and references therein.

(9) Giannini, L.; Caselli, A.; Solari, E.; Floriani, C.; Chiesi-Villa, A.; Rizzoli, C.; Re, N.; Sgamellotti, A. *J. Am. Chem. Soc.* **1997**, *119*, 9198.

4H, ArH), 6.97 (s, 4H, ArH), overlapping with 6.95 (d, J = 9.1 Hz, 4H, ArH), 4.29 (d, J = 12,6 Hz, 4H, *endo*-CH_2), 3.90 (s, 6H, MeO), 3.25 (d, J = 12.6 Hz, 4H, *exo*-CH_2), 2.25 (s, 6H, CH_3), 1.27 (brd, 22H, Bu^t, hexane), 1.10 (s, 18H, Bu^t), 0.89 (m, 3H, hexane). Anal. Calcd for **8**·$(C_6H_{14})_{0.5}$·$(C_6H_6)_{0.5}$, $C_{80}H_{92}O_6Zr$: C, 77.44; H, 7.47. Found: C, 77.39; H, 7.47.

Synthesis of 9. $(Ph)_2CO$ (0.40 g, 2.2 mmol) was added at room temperature to a solution of **13** (1.11g, 1.08 mmol) in toluene (100 mL). A sample of the solution (*ca*. 1 mL) was evaporated to dryness *in vacuo*, and the residue was taken up in C_6D_6. The ^{1}H NMR spectrum of the resulting solution showed the presence of a few extra peaks with respect to that of the isolated product (δ = 7.7 (m, 4H), 7.3−7.05 (m), overlapping with toluene and product peaks, 3.51 (s, 2H), 3.40 (s, 2H), 1.34 (s, 9H)). The same signals were observed for the reaction of **13** with PhCOCOPh, leading to **11**. Volatiles were removed *in vacuo*, hexane was added to the residue, and the white **9** collected and dried *in vacuo* (0.40 g, 33%). ^{1}H NMR (C_6D_6, 298 K): δ 7.96 (m, 8H, ArH, Ph), 7.26 (s, 4H, ArH), 7.09 (m, 8H, ArH, Ph), 6.98 (m, 4H, ArH, Ph), 6.84 (s, 4H, ArH), 4.50 (d, J = 12.4 Hz, 4H, *endo*-CH_2), 3.95 (s, 6H, MeO), 3.22 (d, J = 12.4 Hz, 4H, *exo*-CH_2), 1.45 (s, 18H, Bu^t), 0.80 (s, 18H, Bu^t). Anal. Calcd for **9**, $C_{72}H_{78}O_6Zr$: C, 76.49; H, 6.95. Found: C, 76.32; H, 7.24.

Synthesis of 11. A solution of PhCOCOPh (0.37 g, 1.8 mmol) in toluene (35 mL) was added at room temperature to a solution of **5**·$(C_6H_6)_{1.5}$ (1.90 g, 1.74 mmol) in toluene (100 mL), yielding a greenish solution. Volatiles were removed *in vacuo*, *n*-hexane (40 mL) was added to the residue, and the resulting solution was kept at −24 °C for 2 days. Complex **11**·$(C_6H_{14})_{1.5}$ precipitated as an orange powder, which was collected and dried *in vacuo* (1.5 g, 78%). ^{1}H NMR (C_6D_6, 298 K): δ 8.02 (m, 4H, ArH, Ph), 7.26−7.0 (m, 10H, ArH), 6.78 (s, 4H, ArH), 4.40 (d, J = 12.5 Hz, 4H, *endo*-CH_2), 3.96 (s, 6H, MeO), 3.14 (d, 4H, J = 12.5 Hz, *exo*-CH_2), 1.45 (s, 18H, Bu^t), 1.23 (m, 12H, hexane), 0.88 (m, 9H, hexane), 0.72 (s, 18H, Bu^t). Anal. Calcd for **11**·$(C_6H_{14})_{1.5}$, $C_{69}H_{89}O_6Zr$: C, 74.95; H, 8.11. Found: C, 75.35; H, 7.73. Complex **11** is also obtained through the reaction of **4** and **13** with PhCOCOPh, as shown by ^{1}H NMR spectroscopy.

Synthesis of 12. A solution of Bu^{t}NC (0.74 g, 8.9 mmol) in toluene (50 mL) was added dropwise, at room temperature, to a solution of **1**·C_6H_6 (7.85 g, 8.98 mmol) in toluene (200 mL), to give a yellow solution. After 2 h, volatiles were removed *in vacuo* and hexane (50 mL) was added to the residue. The flask was kept 2 days at −24 °C; the pale yellow **12** was then collected and dried *in vacuo* (5.06 g, 64.0%). ^{1}H NMR (C_6D_6, 298 K): δ 7.21 (s, 4H, ArH), 6.79 (s, 4H, ArH), 4.43 (d, J = 12.4 Hz, 4H, *endo*-CH_2), 4.08 (s, 6H, MeO), 3.15 (d, J = 12.4 Hz, 4H, *exo*-CH_2), 2.14 (s, 6H, Me), 1.74 (s, 9H, NBu^t), 1.45 (s, 18H, Bu^t), 0.86 (s, 18H, Bu^t). Anal. Calcd for **12**, $C_{53}H_{73}O_4NZr$: C, 72.39; H, 8.37; N, 1.59. Found: C, 72.37; H, 8.58; N, 1.50. The product is thermally stable (12 h, 55 °C) but is decomposed in solution by solar light.

Synthesis of 13. Bu^{t}NC (0.38 g, 4.6 mmol) was added at room temperature to a solution of **2** (4.51 g, 4.75 mmol) in toluene (250 mL). After 2 h, a sample of the solution (*ca*. 1 mL) was evaporated to dryness *in vacuo* and the residue was taken up in C_6D_6. The ^{1}H NMR of the resulting solution showed the presence of the starting material together with a small amount of the final product. The IR spectrum of the toluene reaction solution (taken at the same time) coincided with the sum of the IR spectra in toluene of **2** and free Bu^t-NC. After 3 days, volatiles were removed *in vacuo* and *n*-hexane (50 mL) was added to the residue. The flask was kept 14 h at −24 °C; the yellow **13** was then collected and dried *in vacuo* (2.63 g, 53.5%). ^{1}H NMR (C_6D_6, 298 K): δ 7.77 (m, 4H, ArH(PhCH$_2$)), 7.24 (s, 4H, ArH), 7.14 (m, 4H, ArH(PhCH$_2$)), 7.00 (m, 2H, ArH(PhCH$_2$)), 6.75 (s, 4H, ArH), 4.26 (d, J = 12.4 Hz, 4H, *endo*-CH_2), 3.82 (d, J = 15.2 Hz, 2H, PhC*H*$_2$), 3.73 (s, 6H, MeO), 3.68 (d, J = 15.2 Hz, 2H, PhC*H*$_2$), 3.08 (d, J = 12.4 Hz, 4H, *exo*-CH_2), 1.77 (s, 9H, NBu^t), 1.45 (s, 18H, Bu^t), 0.86 (s, 18H, Bu^t).^{1}H NMR (CD_2Cl_2, 298 K): δ 7.64 (m, 4H, ArH-(PhCH$_2$)), 7.14−7.04 (m, 10H, ArH), 6.77 (s, 4H, ArH), 4.20 (d, J = 12.4 Hz, 4H, *endo*-CH_2), 4.02 (s, 6H, MeO), 3.67 (d, J = 15.3 Hz, 2H, PhC*H*$_2$), 3.51 (d, J = 15.3 Hz, 2H, PhC*H*$_2$), 3.16 (d, J = 12.4 Hz, 4H, *exo*-CH_2), 1.70 (s, 9H, NBu^t), 1.35 (s, 18H, Bu^t), 0.96 (s, 18H, Bu^t). Anal. Calcd for **13**, $C_{65}H_{81}O_4NZr$: C, 75.68; H, 7.91; N, 1.36. Found: C, 75.82; H, 8.20; N, 1.13. The symmetry of the spectrum does not change on lowering the temperature to 183 K (broadening only was observed). Crystals suitable for X-ray analysis were obtained at 9 °C from a toluene solution saturated at room temperature. The product is thermally stable (12 h, 55 °C), is decomposed in solution by the action of solar light, and reacts further with Bu^{t}NC to give a complex mixture of products.

Synthesis of 14. A solution of Bu^{t}NC (1.45 g, 17.5 mmol) in benzene (65 mL) was added dropwise at room temperature to a suspension of **1**·C_6H_6 (4.57 g, 5.23 mmol) in benzene (80 mL), and the resulting yellow solution was stirred for 2 h. Volatiles were removed *in vacuo*, and hexane (50 mL) was added to the residue. Yellow **14**·C_6H_6 was then collected and dried *in vacuo* (3.5 g, 59%). ^{1}H NMR (C_6D_6, 298 K): δ 7.37−7.30 (m, 4H, ArH), 6.98−6.89 (m, 4H, ArH), 5.30 (d, J = 12.4 Hz, 1H, CH_2), 4.93 (d, J = 12.0 Hz, 1H, CH_2), 4.74 (d, J = 12.4 Hz, 1H, CH_2), 4.64 (d, J = 12.0 Hz, 1H, CH_2), 4.37 (s, 3H, MeO), 4.01 (s, 3H, MeO), 3.46−3.26 (m, 4H, CH_2), 1.71 (s, 3H, Me), 1.63 (s, 3H, Me), 1.60 (s, 9H, Bu^t), 1.52 (s, 9H, Bu^t), 1.48 (s, 9H, Bu^t), 1.43 (s, 9H, Bu^t), 1.24 (s, 9H, Bu^t), 0.78 (s, 18H, Bu^t). ^{1}H NMR (CD_2Cl_2, 298 K): δ 7.37 (s, 6H, C_6H_6), 7.08−6.98 (m, 8H, ArH), 4.98 (d, J = 12.4 Hz, 1H, CH_2), 4.64 (d, J = 12.0 Hz, 1H, CH_2), 4.53 (s, 3H, MeO), overlapping with 4.48 (d, J = 12.4 Hz, 1H, CH_2), 4.42 (d, J = 12.0 Hz, 1H, CH_2), 4.35 (s, 3H, MeO), 3.32 (d, J = 12.0 Hz, 1H, CH_2), 3.25 (d, 1H, CH_2), overlapping with 3.23 (d, 1H, CH_2), 3.05 (d, J = 12.0 Hz, 1H, CH_2), 1.70 (s, 3H, Me), 1.64 (s, 3H, Me), 1.50 (s, 9H, Bu^t), 1.47 (s, 9H, Bu^t), 1.39 (s, 9H, Bu^t), 1.28 (s, 9H, Bu^t), 1.26 (s, 9H, Bu^t), 1.19 (s, 9H, Bu^t), 1.17 (s, 9H, Bu^t). IR: (Nujol mull) 1965 cm^{-1} (s). Anal. Calcd for **14**·C_6H_6, $C_{69}H_{97}O_4N_3Zr$: C, 73.75; H, 8.70; N, 3.74. Found: C, 73.10; H, 8.55; N, 3.39. Crystals suitable for X-ray analysis were obtained from CH_2Cl_2/hexane solutions kept at −20 °C. The same product can be obtained by adding 2 equiv (or an excess) of Bu^{t}NC to a solution of **12** in toluene or C_6D_6. It is thermally labile (decomposition visible after 8 h at 60 °C in C_6D_6).

Synthesis of 15. A solution of Bu^{t}NC (0.38 g, 4.6 mmol) in toluene (50 mL) was added dropwise to a solution of **1**·C_6H_6 (2.0 g, 2.3 mmol) in toluene (100 mL) at −80 °C. The colorless solution was stirred overnight, while the temperature slowly increased to −5 °C. Volatiles were then removed *in vacuo*, and *n*-hexane (40 mL) was added to the residue. The flask was kept for 1 day at −24 °C; the white **15** was then collected and dried *in vacuo* (1.80 g, 81.8%). ^{1}H NMR (C_6D_6, 298 K): δ 7.31 (d, J = 2.4 Hz, 2H, ArH), 7.29 (d, J = 2.4 Hz, 2H, ArH), 6.97 (d, J = 2.4 Hz, 2H, ArH), 6.93 (d, J = 2.4 Hz, 2H, ArH), 4.72 (d, J = 11.8 Hz, 2H, *endo*-CH_2), 4.40 (d, J = 11.8 Hz, 2H, *endo*-CH_2), 4.12 (s, 6H, MeO), 3.42 (d, 2H, *exo*-CH_2), overlapping with 3.35 (d, 2H, *exo*-CH_2), 2.49 (s, 6H, Me), 1.48 (s, 18H, Bu^t), 1.20 (s, 18H, Bu^t), 0.93 (s, 18H, Bu^t). ^{1}H NMR (CD_2Cl_2, 298 K): δ 6.94−6.89 (m, 8H, ArH), 4.41 (d, J = 11.8 Hz, 2H, *endo*-CH_2), overlapping with 4.34 (s, 6H, MeO), 4.21 (d, J = 11.8 Hz, 2H, *endo*-CH_2), 3.12 (d, 2H, *exo*-CH_2), overlapping with 3.10 (d, 2H, *exo*-CH_2), 2.77 (s, 6H, Me), 1.42 (s, 18H, Bu^t), 1.21 (s, 18H, Bu^t), 1.10 (s, 18H, Bu^t). IR: (Nujol mull) 1585.1 cm^{-1} (m). Anal. Calcd for **15**, $C_{58}H_{82}N_2O_4Zr$: C, 72.38; H, 8.59; N, 2.91. Found: C, 71.90; H, 8.84; N, 2.78. Crystals suitable for X-ray analysis were obtained at −25 °C from a saturated solution in toluene/THF (*ca*. 3:1). The product does not react with excess Bu^t-NC; it is thermally labile both in solution and in the solid state, evolving to the coupled product (*vide infra*).

Synthesis of 16. A solution of Bu^{t}NC (0.49 g, 5.9 mmol) in toluene (25 mL) was added dropwise to a solution of **3** (2.76 g, 2.91 mmol) in toluene (100 mL) at −80 °C. The colorless solution was stirred overnight, while the temperature slowly increased to room temperature. Volatiles were then removed *in vacuo*, and *n*-hexane (50 mL) was added to the residue. The flask was kept 1 day at −24 °C; the white **16**·C_7H_8 was then collected and dried *in vacuo* (1.50 g, 42.7%). ^{1}H NMR (C_6D_6, 298 K): δ 7.42 (d, J = 2.3 Hz, 2H, ArH), 7.37 (d, J = 2.3 Hz, 2H, ArH), 7.15−6.94 (m, ArH), 4.89 (d, J = 11.9 Hz, 2H, *endo*-CH_2), 4.72 (d, J = 11.9 Hz, 2H, *endo*-CH_2), 3.98 (s, 6H, MeO), 3.42 (d, 4H, J = 11.9 Hz, *exo*-CH_2), 2.11 (s, 9H, Me, C_7H_8), 1.49 (s, 18H, Bu^t), 1.35 (s, 18H, Bu^t), 0.89 (s, 18H, Bu^t). ^{1}H NMR (C_6D_6, 298 K): δ 7.60 (d, J = 8.0 Hz, 4H, *p*-MeC_6H_4), 7.36 (s, 4H, ArH), 6.86 (s, 4H, ArH), 6.79 (d, J = 8.0 Hz, 4H, *p*-MeC_6H_4), 4.84 (d, J = 12.4 Hz, 4H, *endo*-CH_2), 3.64 (s, 6H, MeO), 3.37 (d, 4H, J = 12.4 Hz, *exo*-CH_2), 1.97 (s, 6H, Me), 1.48 (s, 36H, Bu^t), 0.94 (s, 18H, Bu^t). Anal. Calcd for **16**·C_7H_8,

Table 1. Experimental Data for the X-ray Diffraction Studies on Crystalline Complexes **5**, **13**−**15**, and **17**

compound	**5**	**13**	**14**	**15**	**17**
formula	$C_{61}H_{72}O_5Zr\cdot 2.5C_6H_6$	$C_{65}H_{81}NO_4Zr\cdot C_7H_8$	$C_{63}H_{91}N_3O_4Zr\cdot 2CH_2Cl_2\cdot 0.5C_6H_{14}$	$C_{58}H_{82}N_2O_4Zr\cdot 2C_7H_8$	$C_{58}H_{92}N_2O_4Zr\cdot C_6H_6$
cryst color	colorless	colorless	pale yellow	colorless	yellow
a (Å)	14.292(3)	18.835(3)	13.691(3)	22.126(3)	13.887(4)
b (Å)	19.206(4)	24.950(4)	20.022(4)	18.562(2)	15.317(5)
c (Å)	12.927(4)	27.151(4)	13.384(3)	17.847(2)	14.973(2)
α (deg)	107.61(2)	90	93.62(2)	90	90
β (deg)	105.00(2)	96.37(1)	105.08(2)	114.99(2)	110.69(2)
γ (deg)	88.25(2)	90	104.44(2)	90	90
V (Å^3)	3262.4(15)	12680.4(34)	3398.3(14)	6643.6(18)	2979.5(14)
Z	2	8	2	4	2
fw	1171.7	1123.7	1258.6	1146.8	1048.7
space group	$P\bar{1}$ (No. 2)	$P2_1/c$ (No. 14)	$P\bar{1}$ (No. 2)	$C2/c$ (No. 15)	$P2_1/m$ (No. 11)
T (°C)	22	−140	−140	−140	22
λ (Å)	1.541 78	1.541 78	1.541 78	1.541 78	0.710 69
ρ_{calcd} (g cm^{-3})	1.193	1.177	1.230	1.146	1.169
μ (cm^{-1})	17.55	17.77	31.71	17.06	2.24
trans coeff	0.812−1.000	0.535−1.000	0.726−1.000	0.647−1.000	0.609−1.000
unique total data	8526 (NO)	22129	12693	5327	5469
unique obsd data	3495	10381 (NO)	5412 (NO)	3713 (NO)	4605 (NO)
R^a	0.069	0.066	0.070	0.058	0.060
w$R2^b$	0.203	0.161	0.167	0.139	0.166
GOF^c	1.106	1.082	1.118	1.063	1.001

[a] $R = \sum|\Delta F|/\sum|F_o|$ calculated on the unique observed data [$I > 2\sigma(I)$]. [b] w$R2 = [\sum w|\Delta F^2|^2/\sum w|F_o^2|^2]^{1/2}$ calculated on the unique observed data for **13**−**15** and **17** and on the unique total data for **5**. [c] GOF $= [\sum w|\Delta F^2|^2/(NO - NV)]^{1/2}$ where NO = number of observed and NV = number of variables.

$C_{77}H_{98}N_2O_4Zr$: C, 76.63; H, 8.18; N, 2.32. Found: C, 76.31; H, 8.49; N, 1.93. The product is thermally labile and evolves to the coupled product **18**.

Synthesis of 17. Solid **15** (1.18 g) was kept at 60 °C in a sealed ampule for 6 days. The solid turned ocre. The reaction was then complete, as shown by ^{1}H NMR. ^{1}H NMR (C_6D_6, 298 K): δ 7.35 (s, 4H, ArH), 6.92 (s, 4H, ArH), 4.58 (d, J = 12.2 Hz, 4H, *endo*-CH_2), 3.52 (s, 6H, MeO), 3.36 (d, 4H, J = 12.2 Hz, *exo*-CH_2), 2.10 (s, 6H, Me), 1.48 (s, 18H, Bu^t), 1.46 (s, 18H, Bu^t), 0.81 (s, 18H, Bu^t). ^{1}H NMR (CD_2Cl_2, 298 K): δ 7.02 (s, 4H, ArH), 6.98 (s, 4H, ArH), 4.31 (d, J = 12.2 Hz, 4H, *endo*-CH_2), 3.87 (s, 6H, MeO), 3.17 (d, J = 12.2 Hz, 4H, *exo*-CH_2), 2.34 (s, 6H, Me), 1.41 (s, 18H, Bu^t), 1.25 (s, 18H, Bu^t), 1.12 (s, 18H, Bu^t). Anal. Calcd for **16**, $C_{58}H_{92}O_4N_2Zr$: C, 72.38; H, 8.59; N, 2.91. Found: C, 72.27; H, 8.80; N, 2.69. In the low-temperature limit, a C_2 symmetric spectrum, although very broad, was obtained. ^{1}H NMR (CD_2Cl_2, 183 K): δ 6.97 (ArH), 6.87 (ArH), 4.50 (d, CH_2), 3.97 (s, MeO), 3.81 (d, CH_2), 3.56 (s, MeO), 3.19 (d, CH_2), 3.05 (d, CH_2), 2.26 (s, Me), 1.30 (s, Bu^t), 1.15 (s, Bu^t), 1.05 (s, Bu^t), 1.00 (s, Bu^t). Crystals suitable for X-ray analysis were obtained at room temperature from a supersaturated benzene solution.

X-ray Crystallography for 5, 13−**15, and 17**. Crystal data and details associated with data collection are listed in Tables 1 and S1 (Supporting Information). Data for all complexes were collected on a single crystal (Rigaku AFC6S) at 295 K for **5** and **17** and at 133 K for **13**−**15**. Structure solutions were based on the observed reflections [$I > 2\sigma(I)$]. The refinements were carried out using the observed reflections for **13**−**15** and **17** and on the unique total reflections for **5**. The structures were solved by the heavy-atom method starting from a three-dimensional Patterson map.[10] Refinements were done by full-matrix minimization of the function $\sum w(\Delta F^2)^2$.[11] In the last stage of refinement, the weighting scheme $w = 1/[\sigma^2(F_o^2) + (aP)^2]$ ($P = (F_o^2 + 2F_c^2)/3$] was applied with a resulting in the value of 0.0781, 0.0954, 0.0779, 0.0561, and 0.1263 for **5**, **13**, **14**, **15**, and **17**, respectively. For complex **5**, refinement was carried out first isotropically and then anisotropically for all non-H atoms. The O5, C48, and C49 atoms of the dibenzyl ketone moiety and the C81−C86 benzene solvent molecule of crystallization were found to be statistically distributed over two positions (A and B), anisotropically refined with site occupation factors of 0.6 and 0.4, respectively. For complex **13**, refinement was done by full-matrix least-squares first isotropically and then anisotropically for all of the non-H atoms. All hydrogen atoms were located from difference Fourier maps and introduced in the subsequent refinements as fixed atom contributions with isotropic U values fixed at 0.08 Å^2. For complex **14**, refinement was done by full-matrix least-squares first isotropically and then anisotropically for all non-H atoms except for some disordered carbon atoms. Some troubles were encountered in refining the structure because the U_{ij} parameters for some Bu^t groups and for the CH_2Cl_2 molecule of crystallization reached rather high values. The best fit was obtained considering the C38−C40 methyl carbons of one calixarene Bu^t group distributed over two positions A (75%) and B (25%) corresponding to different conformations of the butyl group. For complex **15**, refinement was done by full-matrix least-squares first isotropically and then anisotropically for all non-H atoms of the complex molecule. The X-ray analysis revealed the presence of two toluene molecules of crystallization C61···C66 and C71···C74, the former as a guest. Both of them were affected by severe disorder, the guest molecule being disordered about the 2-fold axis running through the complex molecule, the other one being disordered around a crystallographic center of symmetry. For complex **17**, the number of molecules in the unit cell (Z = 2) required the molecules to possess an imposed crystallographic m symmetry in the centrosymmetric $P2_1/m$ space group. The structure was then solved in this space group with the heavy-atom method. The Fourier map calculated with the contribution of the zirconium atom showed the calixarene ligand to be consistent with the presence of the crystallographic mirror implying, by contrast, a statistical distribution of the N−C−C−N fragment about the mirror plane running through the N1 and N2 atoms.

The final difference maps showed no unusual feature, with residual peaks of 0.34, 1.50, 0.77, 0.66, and 0.59 eÅ^{-3} for **5**, **13**−**15**, and **17**, respectively, located along the direction of Zr−O bonds. See the Supporting Information for additional details.

Results

Synthesis and Reactivity. This paper concerns a variety of C−C bond formation reactions assisted by zirconium bonded to a dianionic tetraoxo macrocyclic ligand, *i.e.*, [*p*-Bu^t-calix[4]-$(OMe)_2(O)_2Zr]^{2+}$, hereafter abbreviated as [calix[4]-$(OMe)_2$-$(O)_2Zr]^{2+}$.

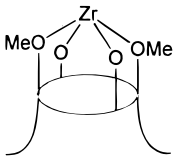

[*p*-Bu^t-calix[4]-$(OMe)_2(O)_2Zr]^{2+}$

(10) Sheldrick, G. M. *SHELX76: Program for Crystal Structure Determination*; University of Cambridge: Cambridge, U.K., 1976.

(11) Sheldrick, G. *SHELXL92: Program for Crystal Structure Refinement*; University of Göttingen: Göttingen, Germany, 1992.

Scheme 1

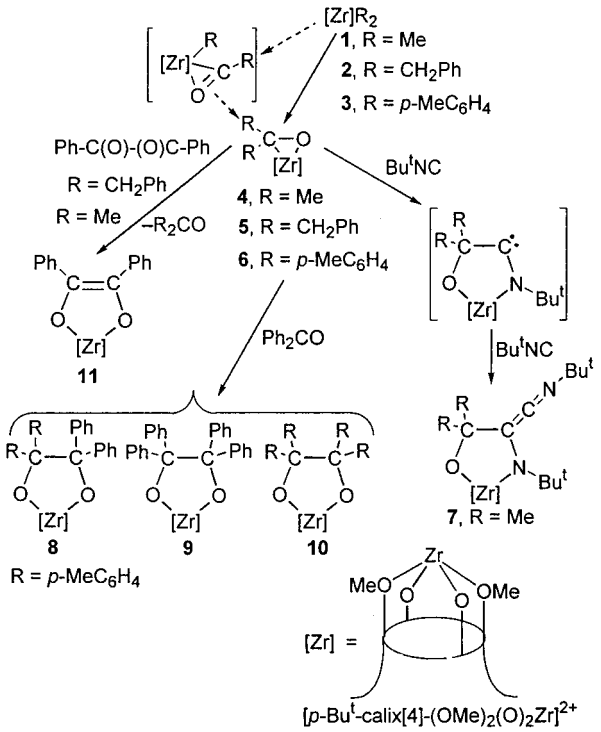

The starting materials of this study are the dialkyl and diaryl derivatives, [calix[4]-$(OMe)_2(O)_2ZrR_2$], whose syntheses and main properties have been reported elsewhere.[9] Such dialkyl and diaryl derivatives undergo a sequential series of insertion reactions occurring with the formation of C−C bonds and giving organic fragments that remain bonded to the calix[4]arene-zirconium moiety. Scheme 1 displays the migratory insertion of carbon monoxide into the Zr−C bonds in **1**−**3** and the further migratory aptitude of the resulting Zr−C functionalities to ketones and isocyanides.

The reaction of **1**−**3** with CO was carried out in benzene at room temperature under 1 atm pressure and was completed in a few minutes. Regardless of the R substituent and the reaction conditions, the η^2-ketones were the only products detected in solution and then isolated as solids. They have been characterized by the conventional analytical methods, including the X-ray analysis on **5** (*vide infra*). The formation of the η^2-ketones **4**−**6** probably occurs *via* the intermediacy of an η^2-acyl, followed by the migration of the second alkyl group to the η^2-acyl carbon.[4] Such a migration is greatly enhanced by the carbenium ion nature of the η^2-acyl.[12] This corresponds to a low-energy vacant π^*_{CO}-accepting orbital. In the present case, unlike when the [ZrR_2] fragment is bonded to the cyclopentadienyl ligand, we were unable to detect the η^2-acyl intermediate.

The higher lability of the Zr−C bond can be associated to the unprecedented, in this kind of complex, six-coordination of the metal (usually it is tetrahedral) and on the topology of the [ZrO_4] fragment. The metal, in such a hemisandwich structure, has, in fact, an open face where it assists the organic transformations of the incoming substrates.

The η^2-metal-bonded ketones **4**−**6** maintain some of the migratory insertion properties typical of the metal−carbon σ-bond.[13] Although no reaction with CO was observed, **4** reacts smoothly with 2 mol of Bu^{t}NC. The formation of **7** can be explained by the sequence shown in Scheme 1. The insertion of Bu^{t}NC on **4** produces a carbenoid metallacycle which then adds the pseudocarbene Bu^{t}NC.[14] The proposed structure for **7** matches all of the analytical and spectroscopic data and is, in addition, supported by the X-ray analysis on the analogous compound **14** (*vide infra*) derived from the insertion of Bu^{t}NC into the η^2-imine derivative **12**. The reaction of η^2-ketone species with a free ketone to form a C−C-coupled diolate, although it is an easy reaction, usually produces a mixture containing the three possible diolate forms, **8**−**10**, derived from the following: (i) the expected cross-coupling reaction, **8**; (ii) the coupling between two incoming ketones, with the contemporary displacement of the previously η^2-coordinated ketone **9**; (iii) the coupling between two originally η^2-metal-bonded ketones **10**. The obtention of such a mixture requires that the η^2-metal-bonded ketone is replaced at an early stage by an incoming ketone, thus both reacting species [Zr(η^2-R_2CO)] and [Zr(η^2-R'_2CO)] can produce the observed mixture. In a single case, we were able to isolate the mixed diolato form **8** (R = *p*-MeC_6H_4) as the unique compound. Significant proof of the displacement of the η^2-metal-bonded ketone is found in the reaction of **4** and **5** with PhCOCOPh to give **11**. In this case, the displacement is followed by a two-electron internal reductive coupling leading to a C=C double bond.

We should emphasize at this stage two results having rare precedents in the literature: (i) the reactivity of the metal−carbon bond in the η^2-metal-bonded ketones **4**−**6** toward inserting groups,[13] a reaction which can be of synthetic utility; (ii) the potential use of **4**−**6** as a source of zirconium(II) in displacement reactions with appropriate substrates.

In the absence of an excessive driving force derived, as in the case of CO, from the oxophilicity of the metal, the reaction with Bu^{t}NC allowed us to better single out almost all of the steps of the migratory insertion of the isocyanide into the Zr−C bonds, as shown in Scheme 2.

The reaction of **1**−**3** with Bu^{t}NC exemplifies the migratory aptitude of the alkyl and aryl groups bonded to zirconium. A complete range of migratory insertion pathways have been observed as a function of the temperature and the nature of R, though only for **1** were we able to select a specific pathway using exclusively temperature as the controlling factor.

The reaction of **1** and **2** with Bu^{t}NC at room temperature using a 1:1 Zr/Bu^{t}NC molar ratio led to the η^2-imine complexes **12** and **13** *via* the intermediacy of the corresponding η^2-iminoacyl.[4,8,15] The migration of the second alkyl group to the η^2-iminoacyl carbon was inferred for **1** and **2** *via* the isolation of the corresponding η^2-imine, while for **3** the corresponding imine occurs with other products (see below). The metal−carbon bond in **12** is still reactive in migration insertion reactions, similar to those observed for the η^2-metal-bonded ketones in **4**−**6**. The reaction of **12** with an excess of Bu^{t}NC or, more simply, the reaction of **1** with 3 mol of Bu^{t}NC at room temperature led to **14**. This reaction implies the preliminary insertion of an isocyanide into the Zr−C bond of the Zr imine

(12) (a) Fanwick, P. E.; Kobriger, L. M.; McMullen, A. K.; Rothwell, I. P. *J. Am. Chem. Soc.* **1986**, *108*, 8095. (b) Arnold, J.; Tilley, T. D.; Rheingold, A. L. *J. Am. Chem. Soc.* **1986**, *108*, 5355. (c) Tatsumi, K.; Nakamura, A.; Hofmann, P.; Stauffert, P.; Hoffmann, R. *J. Am. Chem. Soc.* **1985**, *107*, 4440. (d) Martin, B. D.; Matchett, S. A.; Norton, J. R.; Anderson, O. P. *J. Am. Chem. Soc.* **1985**, *107*, 7952.

(13) (a) Smuck, S.; Erker, G.; Kotila, S. *J. Organomet. Chem.* **1995**, *502*, 75−86. (b) Bendix, M.; Grehl, M.; Fröhlich, K.; Erker, G. *Organometallics* **1994**, *13*, 3366−3369. (c) Erker, G.; Mena, M.; Krüger, C.; Noe, R. *Organometallics* **1991**, *10*, 1201. (d) Erker, G.; Dorf, U.; Czisch, P.; Petersen, J. L. *Organometallics* **1986**, *5*, 668. Erker, G.; Czisch, P.; Schlund, R.; Angermund, K.; Krüger, C. *Angew. Chem., Int. Ed. Engl.* **1986**, *15*, 364.

(14) (a) Valero, C.; Grehl, M.; Wingbermühle, D.; Kloppenburg, L.; Carpenetti, D.; Erker, G.; Petersen, J. *Organometallics* **1994**, *13*, 415. (b) Scott, M. J.; Lippard, S. J. *J. Am. Chem. Soc.* **1997**, *119*, 3411. (c) Ruiz, J.; Vivanco, M.; Floriani, C.; Chiesi-Villa, A.; Rizzoli, C. *Organometallics* **1993**, *12*, 1811−1822 and references therein.

(15) Chamberlain, L. R.; Durfee, L. D.; Fanwick, P. E.; Kobriger, L.; Latesky, S. L.; McMullen, A. K.; Rothwell, I. P.; Folting, K.; Huffman, J. C.; Streib, W. E.; Wang, R. *J. Am. Chem. Soc.* **1987**, *109*, 390−402.

Scheme 2

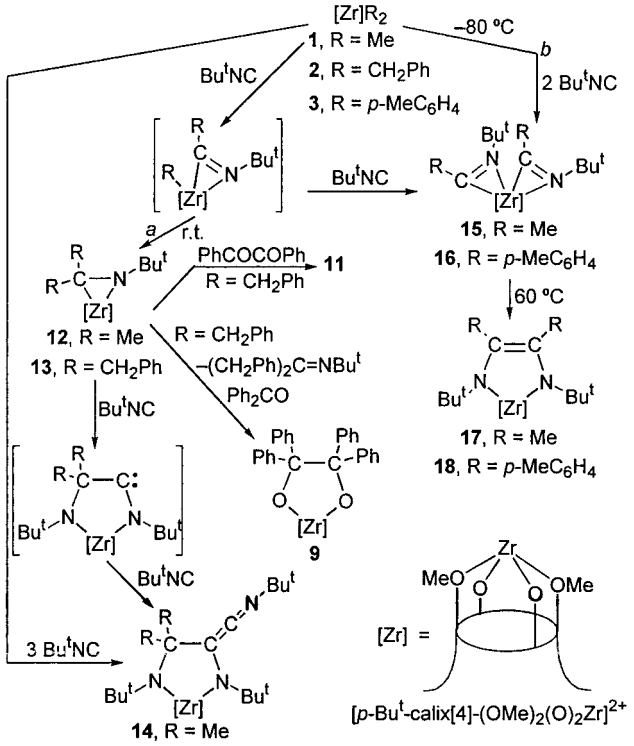

12 to form the carbenoid intermediate, which then adds an additional mole of isocyanide to give **14**.[14] Attempts to insert a ketone into the zirconium−carbon σ bond of the imine **12** resulted, instead, in the displacement of the imine by the ketone, as a consequence of the high oxophilicity of zirconium. The resulting η^2-metal-bonded ketone readily inserts an additional molecule of ketone, thus forming the C−C-coupled product **9**. The proposed displacement of the η^2-metal-bonded imine[16] in **12** and **13** is supported by the identification of the free imine and by the reaction of **13** with PhCOCOPh, leading, as for **4** and **5**, to **11**. These results suggest the possible synthetic utility of **12** and **13** as a source of the $[calix[4]\text{-}(OMe)_2(O)_2Zr]^0$ fragment, formally containing a zirconium(II), more available than **4** and **5**, not containing strongly bonded oxygen donor atoms.

The competitive pathway that has been singled out at low temperature for **1** and **3** (see the Experimental Section) shows the preferential migration of the second alkyl group to an incoming ButNC,[15] to give the bis-η^2-iminoacyls **15** and **16**. Regardless of the Zr/ButNC stoichiometric ratio, the reaction proceeds *via* pathway b at low temperature for **1** and **3**, while for **2**, which is unreactive at low temperature, the only compound formed at room temperature, *via* pathway a, is **13**. For the *p*-tolyl substituent, pathway b is preferred, since we observe only very limited formation of the η^2-imine even under forced conditions. Gentle heating (60 °C) induces the intramolecular coupling[17] of the two η^2-iminoacyl derivatives **15** and **16** to the corresponding enediamido complexes **17** and **18**. The rate, the mechanism, and the theoretical treatment of such an intramolecular coupling of the η^2-iminoacyls **15** and **16** will be discussed in the next section.

Structural Studies. Details of the synthesis and characterization of all of the compounds listed in Schemes 1 and 2 are reported in the Experimental Section. The X-ray analysis has been performed on the prototype of each class, namely, **5**, **13**−**15**, and **17**.

(a) NMR Analysis. The NMR structural studies have mainly focused on the possibility of stressing a solid state−solution structural relationship and on the attempt to use parts of the calix[4]arene, namely, the methylenes, the methyls from the methoxy, or the *p*-But groups, as spectroscopic probes for inspecting the symmetry and the bonding mode of the organometallic fragments bound to the lower rim of the calix. A guideline in this context will be discovering that we can shape the calix[4]arene cavity using the changes in the coordination number of the metal. In Table 2 the chemical shifts of the various fragments of the calix[4]arene skeleton are listed according to the organic moiety bonded to the metal on the open face of the molecule, dedicated to the metal-assisted reactivity. The chemical shift patterns for But, MeO, and bridging methylenes reveal the symmetry of the metal−calix[4]arene moiety as a function of the fragment attached to the metal: (i) 2 singlets (But), 1 pair of doublets ($>CH_2$), 1 singlet (MeO) for a C_{2v} symmetry; (ii) 2 singlets (But), 2 pairs of doublets ($>CH_2$), 1 singlet (MeO) for a C_2 symmetry; (iii) 3 singlets (But), 2 pairs of doublets ($>CH_2$), 1 or 2 singlets (MeO) for a C_s symmetry; (iv) 4 singlets (But), 4 pairs of doublets ($>CH_2$), 2 singlets (MeO) for a C_1 symmetry. For **7** and **14**−**16**, the symmetry of the spectra coincides with that revealed by the X-ray analysis. For complexes **1**−**6**, **8**−**11**, **17**, and **18**, the symmetry observed in solution is slightly higher than the crystallographic one and corresponds to an "idealized structure". The discrepancy can be ascribed to the absence in solution of solid state effects and to a modest degree of fluxionality. On the other hand, complexes **12** and **13** show an apparent C_{2v} symmetry (which is impossible for any conformation reasonably accessible by these complexes), revealing an extreme fluxionality that cannot be "frozen" even at low temperature (193 K).

(b) X-ray Analysis. Complex **5** (Figure 1) crystallizes with 2.5 molecules of benzene, one of them hosted in the calix[4]arene cavity. Complex **13** (Figure 2) crystallizes with one molecule of toluene out of the cavity. In the unit cell of **13**, there are two crystallographically independent molecules (A and B), which have very close parameters. The values referred to molecule B are given in Table 3, but not mentioned in the text. Complex **14** (Figure 3) crystallizes with CH_2Cl_2 and *n*-hexane in the 1:2:0.5 molar ratio, and one of the CH_2Cl_2 molecules is hosted in the calix[4]arene cavity. Complex **15** (Figure 4) crystallizes with 2 molecules of toluene, one of them hosted in the calix[4]arene cavity. Complex **17** (Figure 5) crystallizes with 1 molecule of benzene as a guest. For reasons of conciseness and clarity, the overall structures have been examined according to common and noncommon fragments.

(i) The Calix[4]arenezirconium Moiety. In all of the complexes **5**, **13**−**15**, and **17** (Figures 1−5 and Tables 3 and 4), the hexacoordination of the metal and the differences in the Zr−O bond distances and angles greatly distort the O_4 core from the planarity, typical of the cone conformation of the calix[4]arene. In particular, the rather short Zr−O1 and Zr−O3 bond distances along with the wide bond angles that are close to linear, Zr−O1−C1 and Zr−O3−C10 reveal a Zr−O multiple bond,[15,17,18] while zirconium interacts with O2 and O4 via a normal single bond. The calixarene ligand assumes a slightly flattened cone conformation with the opposite A and C rings pushed outward and the opposite B and D rings toward the cavity of the macrocycle, as indicated by the dihedral angles they form with the "reference plane" through the methylene

(16) (a) Durfee, L. D.; Hill, J. E.; Kerschner, J. L.; Fanwick, P. E.; Rothwell, I. P. *Inorg. Chem.* **1989**, *28*, 3095−6. (b) Durfee, L. D.; Fanwick, P. E.; Rothwell, I. P. Folting, K.; Huffmann, J. C. *J. Am. Chem. Soc.* **1987**, *109*, 4720−2.

(17) Chamberlain, L. R.; Durfee, L. D.; Fanwick, P. E.; Kobriger, L. M.; Latesky, S. L.; McMullen, A. K.; Steffey, B. D.; Rothwell, I. P.; Folting, K.; Huffman, J. C. *J. Am. Chem. Soc.* **1987**, *109*, 6068−6076.

(18) Latesky, S. L.; McMullen, A. K.; Niccolai, G. P.; Rothwell, I. P. *Organometallics* **1985**, *4*, 902.

Table 2. Chemical Shifts of **1**−**18** in C_6D_6 at 298 K

cmpd	Bu^t	MeO	*exo*-CH_2	*endo*-CH_2	ΔCH_2	*J* (Hz)	sym
1	1.46, 0.77	3.69	3.18	4.46	1.28	12.5	C_{2v}
2	1.45, 0.70	3.37	3.24	4.46	1.22	12.5	C_{2v}
3	1.44, 0.84	3.35	3.19	4.60	1.41	12.5	C_{2v}
4	1.45, 0.74, 0.77	4.43, 4.20	3.15, 3.27	4.42, 4.45	(1.22)	12.5	C_s
5	1.44, 0.72, 0.74	4.45, 4.03	3.19, 3.18	4.22	1.03	12.4	C_s
6	1.39, 0.75, 0.68	4.47, 4.32	3.15	4.43	1.32	12.4	C_s
7	1.44, 0.69, 1.46, 0.73	4.11, 4.0	∼3.4−3.2	4.4−4.6	∼1.2	∼12.5	C_1
8	1.10, 1.27	3.90	3.25	4.29	1.04	12.6	C_{2v}
9	1.45, 0.80	3.95	3.22	4.50	1.28	12.4	C_{2v}
11	1.45, 0.72	3.96	3.14	4.40	1.26	12.5	C_{2v}
12	1.45, 0.86	4.08	3.15	4.43	1.28	12.4	C_{2v}
13	1.45, 0.86	3.73	3.08	4.26	1.18	12.4	C_{2v}
14	1.48, 0.78, 1.43	4.37, 4.01	3.46−3.26	4.64, 4.93, 4.74, 5.3	2−1.3	12.0, 12.4	C_1
15	1.48, 0.93	4.12	3.35, 3.42	4.40, 4.72	(1.27)	11.8	C_2
16	1.49, 0.89	3.98	3.42	4.72, 4.89	1.43	11.9	C_2
17	1.48, 0.81	3.52	3.36	4.58	1.22	12.2	C_{2v}
18	1.48, 0.94	3.64	3.37	4.84	1.47	12.4	C_{2v}

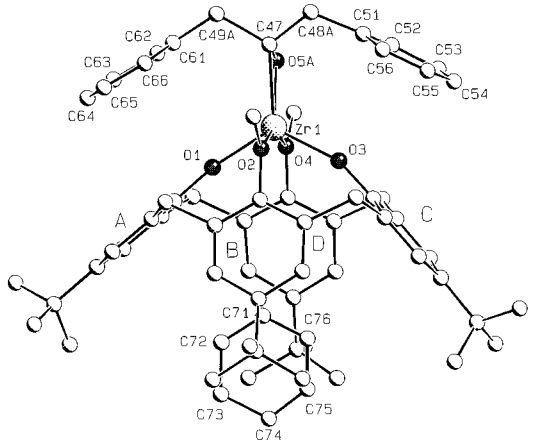

Figure 1. A SCHAKAL view of complex **5**. Disorder has been omitted for clarity.

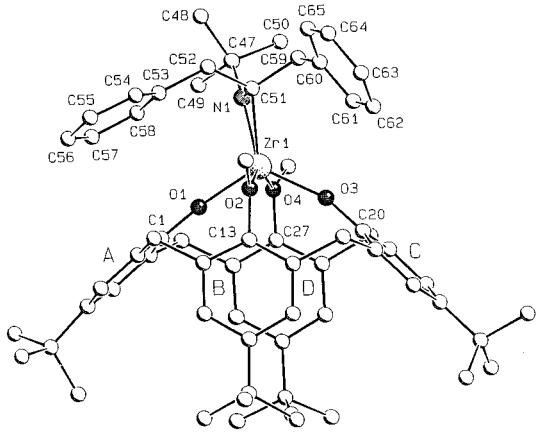

Figure 2. A SCHAKAL view of molecule A of complex **13**.

carbon atoms C7, C14, C21, and C28 (Scheme 3, Table 5a). The elliptical section of the cavity is indicated by the distances between opposite *p*-carbon atoms (Table 5b). The most pronounced ellipticity of the cavity is observed for complex **13**, as evidenced by the short C10···C24 distance [5.740(10) Å] and the high B∧D angle (Table 5). As already observed in similar cases,[9] solvent inclusion is impossible in such an elliptical cavity, and in fact, complex **13** is the only one to crystallize without a guest molecule.

(ii) The Guest Solvent. Complex 5. The C71···C76 guest benzene molecule enters the cavity of the complex molecule with its C71···C74 axis along the molecular axis, as indicated by the value of the Zr···C71···C74 angle (173.3(8)°). The Zr···C71 distance of 5.03(2) Å rules out any possible Zr···H interaction. The guest molecule is oriented nearly parallel to the B and D rings (dihedral angles 19.9(6) and 18.6(6)°, respectively) and perpendicular to the A and C rings (dihedral angles 87.0(5) and 87.6(6)°, respectively). The host−guest interactions could be interpreted in terms of CH_3/π interactions[19] occurring between the protons of the methyl groups of the host and the guest aromatic ring, as is inferred from the following distances: C34···C75, 3.82(3) Å; H342···C75, 2.70 Å; C35···C73, 3.92(3) Å; H352···C73, 2.69 Å; C42···C75, 3.73(3) Å; H422···C75, 2.58 Å; C43···C73, 3.80(4) Å; H432···C73, 2.67 Å.

Table 3. Selected Bond Distances (Å) and Angles (deg) for Complexes **5** and **13**

Complex **5**			
Zr1−O1	1.966(6)	Zr1−O5A	2.084(11)
Zr1−O2	2.323(8)	Zr1−C47	2.210(12)
Zr1−O3	1.966(6)	O5A−C47	1.32(2)
Zr1−O4	2.314(7)		
O5A−Zr1−C47	35.5(4)	Zr1−O4−C27	118.2(5)
O2−Zr1−O4	153.1(3)	Zr1−O5A−C47	77.5(8)
O1−Zr1−O3	120.2(3)	Zr1−O5B−C47	77.4(9)
Zr1−O1−C1	171.6(6)	Zr1−C47−O5B	69.4(9)
Zr1−O2−C13	119.3(6)	Zr1−C47−O5A	67.0(7)
Zr1−O3−C20	159.0(6)		

Complex **13**		
	molecule A	molecule B
Zr1−O1	1.967(6)	1.960(6)
Zr1−O2	2.355(5)	2.339(5)
Zr1−O3	2.020(5)	2.026(5)
Zr1−O4	2.466(6)	2.527(6)
Zr1−N1	2.048(7)	2.043(7)
Zr1−C51	2.261(8)	2.281(8)
N1−C47	1.482(12)	1.467(11)
N1−C51	1.434(11)	1.425(9)
N1−Zr1−C51	38.5(3)	38.0(3)
O2−Zr1−O4	150.3(2)	150.1(2)
O1−Zr1−O3	120.4(2)	120.2(2)
Zr1−O1−C1	174.6(5)	173.9(5)
Zr1−O2−C13	115.0(4)	114.6(4)
Zr1−O3−C20	162.0(5)	163.0(5)
Zr1−O4−C27	110.2(4)	109.5(4)
Zr1−N1−C51	78.8(4)	80.1(4)
C47−N1−C51	127.5(7)	127.5(7)
Zr1−C51−N1	62.7(4)	61.9(4)

Complex 14. One CH_2Cl_2 solvent molecule is hosted in the calixarene cavity. It is oriented nearly parallel to the B and D rings (dihedral angles 22.4(7) and 25.2(5)°, respectively) and perpendicular to the A and C rings (dihedral angles 88.1(7) and

(19) Andreetti, G. D.; Ugozzoli, F. In ref 1b, pp 88−122.

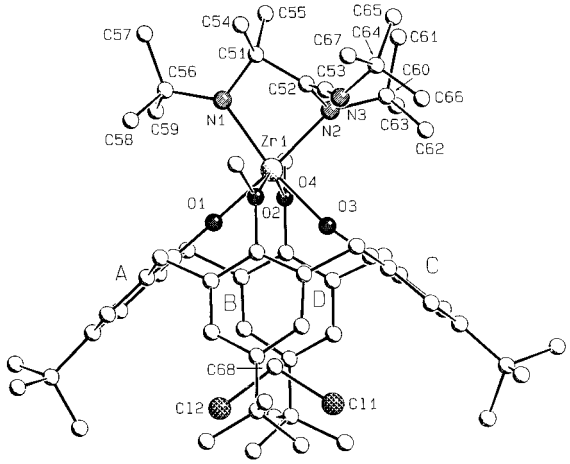

Figure 3. A SCHAKAL view of complex **14**. Disorder has been omitted for clarity.

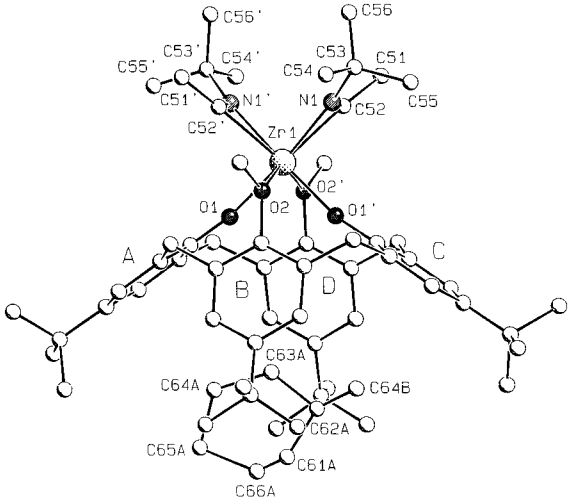

Figure 4. A SCHAKAL view of complex **15**. Prime denotes a transformation of $-x, y, 0.5 - z$. Disorder has been omitted for clarity.

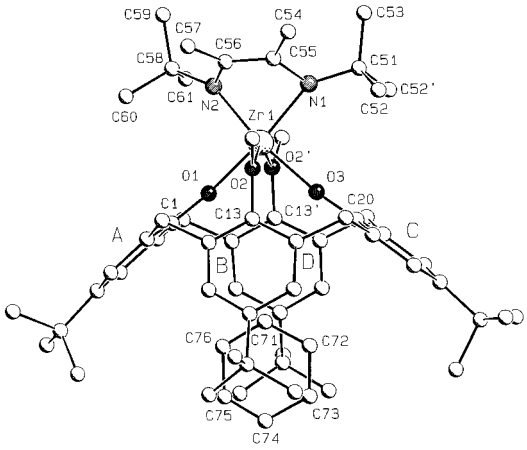

Figure 5. A SCHAKAL view of complex **17**. Prime denotes a transformation of $x, 0.5 - y, z$. Disorder has been omitted for clarity.

86.0(5)°, respectively), so as to orientate the hydrogen atoms toward the center of the B and D rings (CT1···C68, 3.397(12) Å; CT2···C68, 3.520(16) Å; H682···CT1, 2.45 Å; CT2···H681, 2.57 Å; CT1 and CT2 refer to the centroids of the B and D rings, respectively).

Complex 15. The macrocycle shows an elliptical cone conformation more symmetric than those observed for complexes **5** and **13** (Table 5 and above). The toluene molecule enters the cavity not aligning its molecular axis with that of the complex, resulting in a statistical distribution of the molecule around the 2-fold axis. The disorder prevents any sound discussion on the nature of interactions with calixarene. The mean plane through the disordered positions forms dihedral angles of 18.7(1)° with the symmetry-related B and D rings.

Table 4. Selected Bond Distances (Å) and Angles (deg) for Complexes **14**, **15**, and **17**

	Complex **14**		
Zr1−O1	2.014(7)	N1−C51	1.488(13)
Zr1−O2	2.373(6)	N2−C52	1.443(11)
Zr1−O3	2.025(8)	N3−C53	1.227(14)
Zr1−O4	2.364(5)	C51−C52	1.526(16)
Zr1−N1	2.154(9)	C52−C53	1.324(15)
Zr1−N2	2.159(9)		
N1−Zr1−N2	82.1(3)	Zr1−N2−C52	83.3(5)
O2−Zr1−O4	146.2(3)	C53−N3−C64	130.0(10)
O1−Zr1−O3	95.3(3)	N3−C53−C52	175.5(11)
Zr1−O1−C1	178.3(6)	Zr1−O3−C20	171.0(6)
Zr1−O2−C13	121.6(5)	N1−C51−C52	100.0(8)
Zr1−O4−C27	122.1(5)	N2−C52−C51	117.5(8)
Zr1−N1−C51	107.1(6)	C51−C52−C53	120.4(9)
		N2−C52−C53	121.6(10)
	Complex **15**		
Zr1−O1	2.054(4)	Zr1−C52	2.259(6)
Zr1−O2	2.450(5)	N1−C52	1.271(8)
Zr1−N1	2.249(4)		
N1−Zr1−C52	32.7(2)	Zr1−O2−C13	120.0(3)
O1−Zr1−O1′ [a]	91.9(1)	Zr1−N1−C52	74.0(3)
O2−Zr1−O2′	143.8(1)	Zr1−C52−N1	73.2(3)
Zr1−O1−C1	169.4(4)		
	Complex **17**		
Zr1−O1	2.031(5)	Zr1−N2	2.097(7)
Zr1−O2	2.401(3)	N1−C55	1.507(9)
Zr1−O3	2.037(4)	N2−C56	1.450(15)
Zr1−N1	2.104(7)	C55−C56	1.385(13)
N1−Zr1−N2	80.4(3)	Zr1−O3−C20	173.1(4)
O2−Zr1−O2″ [b]	146.2(1)	Zr1−N1−C55	90.3(4)
O1−Zr1−O3	94.5(2)	Zr1−N2−C56	89.5(6)
Zr1−O1−C1	174.4(4)	N2−C56−C55	118.6(9)
Zr1−O2−C13	120.7(2)		

[a] Prime denotes a transformation of $-x, y, 0.5 - z$. [b] Prime denotes a transformation of $x, 0.5 - y, z$.

Scheme 3

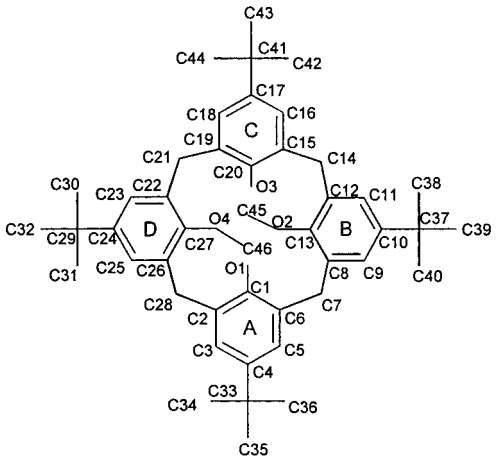

Complex 17. The C71···C76 guest benzene molecule lying on the mirror plane enters the cavity aligning the C71···C74 axis along the molecular axis of the complex, as indicated by the value of the Zr···C71···C74 angle (178.8(7)°). The molecule is perpendicular from symmetry requirements to the A and C rings and nearly parallel to the B and D rings (dihedral angle 19.9(5)°). The host−guest interactions are of the same kind as those observed in complex **5**, the shortest contacts involving the C34 methyl carbon of the host and the C74, C75 carbon atoms of the guest are C34···C74, 3.989(9) Å;

Table 5. Comparison of Selected Dihedral Angles for Complexes **5**, **13**−**15**, and **17**

(a) Dihedral Angles (deg) between Planar Moieties[a]

	5	**13**[b]		**14**	**15**	**17**
E∧**A**	140.7(2)	139.4(2)	[138.8(2)]	138.5(2)	145.4(2)	139.3(1)
E∧**B**	110.2(2)	100.1(2)	[97.5(2)]	110.6(2)	108.6(2)	109.9(1)
E∧**C**	130.5(2)	136.3(2)	[138.1(2)]	142.1(2)	145.4(2)	141.6(1)
E∧**D**	108.2(2)	94.1(3)	[95.4(2)]	108.7(2)	108.6(2)	109.9(1)
A∧**C**	91.2(2)	95.8(3)	[96.9(3)]	100.6(3)	110.8(2)	100.9(1)
B∧**D**	141.6(3)	165.8(2)	[167.1(2)]	140.7(3)	142.7(2)	140.2(2)

(b) Contact Distances (Å) between *p*-Carbon Atoms of Opposite Aromatic Rings[c]

	5	**13**	**14**	**15**	**17**
C4···C17	9.294(12)	9.652(11)	9.472(15)	9.835(10)	9.508(8)
C10···C24	7.096(12)	5.740(10)	7.154(12)	7.044(10)	7.171(7)

[a] The **E** reference plane refers to the least-squares mean plane defined by the C7, C14, C21, and C28 bridging methylenic carbons. [b] Values in square brackets refer to molecule B. [c] In complex **15**, C17 and C24 should be read C4′ and C10′, respectively (the prime = $-x$, y, $0.5 - z$). In complex **17**, C24 should be read C10′ (the prime = x, $0.5 - y$, z).

H341···C74, 3.05 Å; C34···C75, 3.753(9) Å; and H341···C75, 2.81 Å. The Zr···C71 distance is 4.947(8) Å (Zr···H71, 4.02 Å).

(iii) The Organic Fragment Bonded to Zirconium. Complex 5. In spite of the disorder involving the O5 oxygen atom, the values of the Zr−O5 and Zr−C47 bond distances are consistent with an asymmetric η^2-C,O interaction of the dibenzyl ketone to zirconium [Zr−O5A, 2.084(11) Å; Zr−O5B, 2.119(17) Å; Zr−C47, 2.210(12) Å]. The O5−C47 bond distance (O5A−C47, 1.32(2) Å; O5B−C47, 1.24(2) Å) due to the molecular disorder does not have a correct estimation.

Complex 13. The η^2-bonded imine shows an asymmetric bonding mode to the metal, the Zr−N1 and Zr−C51 bond distances being 2.048(7) [2.043(7)] and 2.261(8) [2.281(8)] Å, respectively. The N1−C51 bond distance [1.434(11) Å] is, as expected, consistent with a single bond.[16b]

Complex 14. The parameters listed in Table 4 support the structure drawn for **14**, and rule out any interaction of the metal with the cumulene C52−C53−N3 moiety. The organic fragment acts as an enediamido ligand. The Zr, N1, C51, C52, and N2 five-membered chelate ring assumes an envelope conformation with the N2 atom protruding by 1.049(8) Å from the plane through Zr, N1, C51, and C52.

Complex 15. The two η^2-iminoacyl groups are η^2-bonded to zirconium, in a *trans* arrangement, as is found in the few cases of bis-η^2-iminoacyls reported thus far, with very close Zr−C and Zr−N bond distances [Zr1−N1, 2.249(4) Å; Zr1−C52, 2.259(6) Å]. The N1−C52 bond distance [1.271(8) Å] is in agreement with a double bond.[15]

Complex 17. The enediamido[17] ligand forms a metallacycle which is nearly planar and forms a dihedral angle of 31.8(3)° with the reference plane. The complex possesses a crystallographically imposed *m* symmetry with the mirror plane running through Zr, O1, O3, N1, and C51. This requires a statistical distribution of the N2 and C54···C61 atoms over two positions about the mirror plane.

Discussion

All reactions displayed in Schemes 1 and 2 belong to four general classes, namely: (i) the migratory insertion of carbon monoxide or isocyanides into a metal−alkyl bond with the consequent formation of η^2-acyl or η^2-iminoacyl functionalities; (ii) the alkyl-/aryl- migration to an η^2-acyl or η^2-iminoacyl metal-bonded moiety, leading to the corresponding η^2-ketone or η^2-imine; (iii) the intramolecular coupling of two η^2-iminoacyls to an enediamido ligand; (iv) the migratory insertion of ketones and isocyanides into the M−C bond of η^2-metal-bonded ketones and imines.

The discussion will essentially focus on the kinetic study and on the mechanistic and theoretical interpretation of some aspects of the migratory insertion of carbon monoxide (see the formation of η^2-metal-bonded ketones in Scheme 1) and isocyanides (see the formation of η^2-metal bonded imines, η^2-iminoacyls, and their coupling in Scheme 2) into the Zr−C bonds of complexes **1**−**3**.

The Kinetic Study of the η^2-Iminoacyl Coupling. As far as the mechanistic interpretation of the η^2-iminoacyl coupling reaction is concerned, we refer, as a guideline, to the fundamental work by Rothwell.[20]

The rates of conversion of **15** and **16** into **17** and **18**, respectively, were obtained by ^{1}H NMR measurements, as reported in the Supporting Information. The intramolecular coupling followed first-order kinetics in both cases. The activation parameters [$\Delta H^{\ddagger}$ (kJ mol^{-1}), E_a (kJ mol^{-1})] obtained from the kinetic measurements are, respectively, 106 ± 2, 109 ± 2 for complex **15** and 113 ± 8, 116 ± 8 for complex **16**.

Although in our compounds we are dealing with a pseudo-octahedral coordination of the metal, this does not seem to have a significant impact on the energy pathway of the coupling. Our parameters are, in fact, very close to those of Rothwell, as is our mechanistic interpretation (*vide infra*).[20]

Theoretical Interpretation of the Migratory Insertion Reaction of CO and RNC. Extended Hückel calculations[21,22] have been performed with the aim of understanding the major differences which exist between the $[Cp_2Zr]^{2+}$ and the $[calix[4]\text{-}(OMe)_2(O)_2Zr]^{2+}$ fragments in driving the migratory insertion of carbon monoxide and isocyanides into the metal−carbon bonds of the $[ZrR_2]$ functionality. To this purpose, we examine in detail, emphasizing the major differences between CO and RNC, the following items: (i) the formation of the η^2-metal-bonded acyl and its conversion to η^2-ketone; (ii) the formation of the η^2-bonded iminoacyl and either its transformation in η^2-imine or its reductive coupling to the enediamido.

The $[calix[4]\text{-}(OMe)_2(O)_2Zr]^{2+}$ fragment has already been considered from a theoretical point of view,[9] and its frontier orbitals are depicted in Figure 6, where we report, for comparison, the five metal-based empty orbitals of $[Cp_2Zr]^{2+}$.

The two lowest frontier orbitals of $[Cp_2Zr]^{2+}$ ($1a_1$ and $1b_1$) have the same symmetry properties of those of the $[calix[4]\text{-}(OMe)_2(O)_2Zr]^{2+}$. However, while the former fragment has only another low-lying empty orbital ($2a_1$) available for bonding with additional ligands, the latter fragment has two ($1b_2$, $1a_2$), and this has important consequences on its chemical behavior.

(20) Durfee, L. D.; McMullen, A. K.; Rothwell, I. P. *J. Am. Chem. Soc.* **1988**, *110*, 1463−1467 and references therein.
(21) Hoffmann, R.; Lipscomb, W. N. *J. Chem. Phys.* **1962**, *36*, 2179.
(22) Hoffmann, R. *J. Chem. Phys.* **1963**, *39*, 1397.

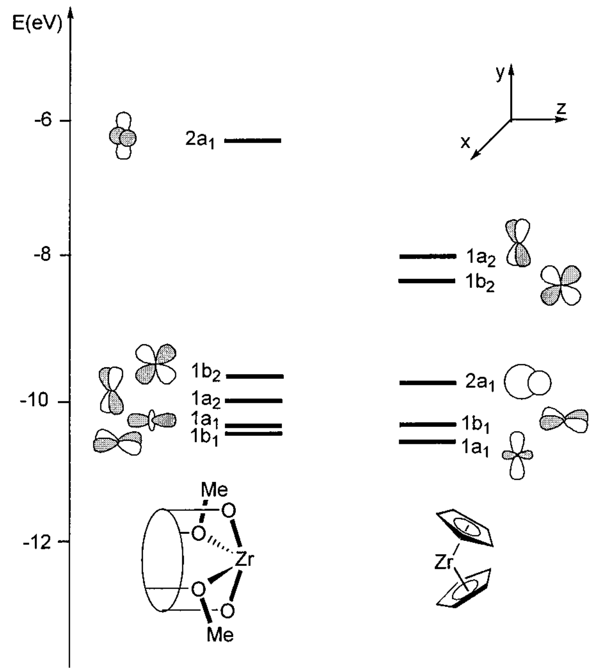

Figure 6. Frontier orbitals of the $[calix[4](OMe)_2(O)_2Zr]^{2+}$ fragment (left), compared with the $[Cp_2Zr]^{2+}$ fragment (right).

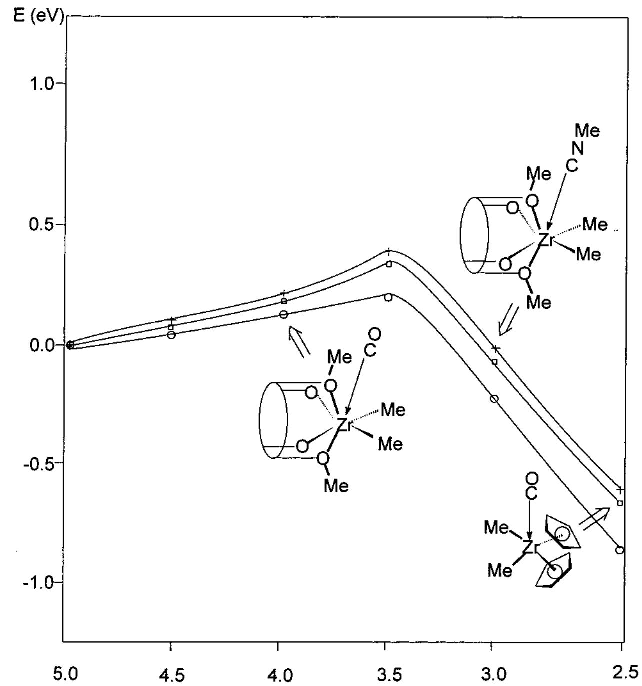

Figure 7. Total energy profiles for the CO approach toward $[calix[4](OMe)_2(O)_2ZrMe_2]$ and $[Cp_2ZrMe_2]$, and the CNMe approach to $[calix[4](OMe)_2(O)_2ZrMe_2]$.

Scheme 4

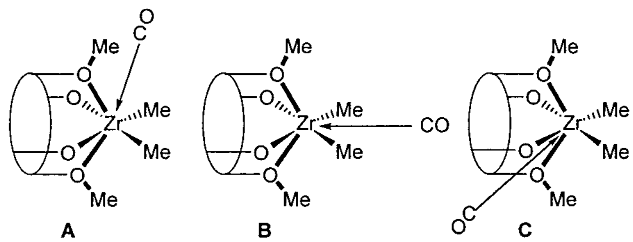

First, these four low-lying d-orbitals can accommodate up to eight electrons, and this is fully exploited in the bis-η^2-iminoacyl compounds **15** and **16**. This behavior is at variance with that of $[Cp_2Zr]^{2+}$ which can accommodate a maximum of six electrons without violating the effective atomic number (EAN) rule. Moreover, while in $[Cp_2Zr]^{2+}$ all of the three low-lying frontier orbitals lie in the symmetry plane bisecting the Cp−Zr−Cp angle (*xz*); in $[calix[4]\text{-}(OMe)_2(O)_2Zr]^{2+}$ only two out of the four lowest-lying orbitals are coplanar, thus favoring a facial over a meridional structure when such a fragment is bound to three additional ligands.

In the hexacoordinate $[calix[4]\text{-}(OMe)_2(O)_2ZrR_2]$ compounds, **1**−**3**, the two alkyl groups lie in the *yz* plane. Only two of the low-lying d-orbitals are used, notably $1a_1$ and $1b_2$ (d_{yz}) which interact, respectively, with the in-phase and out-of-phase combinations of the two σ orbitals of the alkyl groups, leaving as LUMO the $1b_1(d_{xz})$ orbital. Its spatial extension suggests that the most favorable approach of the CO or Bu^tNC nucleophilic species occurs along a line in the *xz* plane forming an angle of approximately 45° with the *z*-axis. We first simulated the initial stages of the CO attack by performing extended Hückel calculations on the $[calix[4]\text{-}(OMe)_2(O)_2ZrMe_2]\cdots CO$ system with different CO to metal distances, from 5.0 to 2.5 Å, along three possible directions, *i.e.*, a line in the *xz* plane forming an angle of approximately 45° with the *z*-axis, a line in the *yz* plane bisecting the Me−Zr−Me angle, and a line in the *yz* plane perpendicular to the z-axis, respectively, **A**, **B**, and **C** in Scheme 4. For the first two approaches, we relaxed the Me−Zr−Me angle at each point along the attack pathway; for the second approach, we also relaxed the dihedral angle between Me−Zr−Me and O−Zr−O planes and the angular position of CO, while in the third approach we independently relaxed the angles of the two Me groups and of CO. It was discovered that pathway **A** is by far energetically more favorable than **B** and **C** (with a barrier of only *ca*. 0.2 eV *vs* 2.2 and 2.4 eV, respectively). The total energy profile for approach **A** is compared in Figure 7 with that for the approach of CO toward $[Cp_2ZrR_2]$ (for which a **C**-like approach is known to be the most favorable).[12c] We see that the energy barrier for $[calix[4]\text{-}(OMe)_2(O)_2ZrMe_2]$ is slightly lower than for $[Cp_2ZrR_2]$, with the corresponding precoordinated CO complex always lower in energy. This suggests a more electrophilic character of the $[calix[4]\text{-}(OMe)_2(O)_2Zr]^{2+}$ *vs* $[Cp_2Zr]^{2+}$, in agreement with the Mulliken charges calculated on the zirconium atom (+2.1 and +1.5, respectively).

Scheme 5

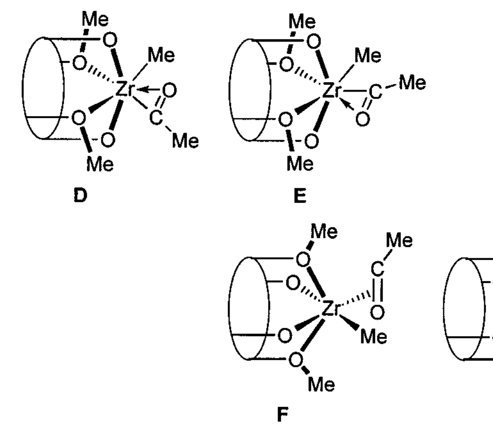

We then considered the hypothetical η^2-acyl intermediate $[calix[4]\text{-}(OMe)_2(O)_2Zr(\eta^2\text{-}MeCO)(Me)]$ in the three possible idealized structures (**D**, **E**, and **F**), and in a plausible η^1-acyl geometry, **G**, as shown in Scheme 5.

Previous calculations[12c] on the analogous $[Cp_2Zr(\eta^2\text{-}MeCO)(Me)]$ species have taken into account only structures **D** and **E** with the η^2 planar moiety lying in the equatorial plane, the only experimentally observed for these bis-cyclopentadienyl systems, showing that the O-inside structure **D** is more stable by *ca*. 0.2

eV. In those calculations, the η^1-acyl geometry **G** was also proposed as an intermediate in the isomerization pathway between **D** and **E** and was calculated to be less stable than **D** by *ca*. 0.4 eV. In our calculations on [calix[4]-$(OMe)_2(O)_2$Zr-(η^2-MeCO)(Me)], we fixed the Zr−C(methyl), Zr−C(acyl), and C−O distances (2.30, 2.21, and 1.29 Å, respectively) and the C(acyl)−O−C angle (120°) and optimized the Zr−C−O and the C(methyl)−Zr−C(acyl) angles, α and β in Scheme 5. The results have shown that the most stable structure is **F**, with the η^2 planar moiety lying perpendicular to the *yz* plane. Moreover, when we constrained the acyl moiety to lie in the equatorial plane, we found the η^1 geometry **G** more stable than the η^2 geometries **D** or **E** (*ca*. 1 eV higher than **C**). Note that the most stable structure **F** found in these calculations has the same geometry experimentally observed in the X-ray analysis for the η^2-iminoacyl moieties in the bis-η^2-iminoacyl complex **15**. The different geometries calculated for [calix[4]-$(OMe)_2(O)_2$Zr(η^2-MeCO)(Me)] and [Cp_2Zr(η^2-MeCO)(Me)] can be rationalized in terms of plausible interactions between the frontier orbitals of each metal fragment and the acetyl moiety. For the [Cp_2-Zr]$^{2+}$ fragment, only orbitals in the equatorial plane are available, thus ruling out nonplanar structures such as **F**, while for [calix[4]-$(OMe)_2(O)_2$Zr]$^{2+}$ there are vacant low-energy orbitals lying on both the perpendicular symmetry planes, suggesting that species with three additional ligands are not stable in a meridional geometry (such as **D** or **E**).

A comparison of the orbital energies of [calix[4]-$(OMe)_2$-$(O)_2$Zr(η^2-MeCO)(Me)] and [Cp_2Zr(η^2-MeCO)(Me)] aids in the explanation of the fast migration, in the former hypothetical species, of the second alkyl leading to the η^2-ketone complex. Hoffmann and co-workers have shown that the reactivity of such an η^2-coordinated acyl can be described in terms of a ''carbenium-type'' character and is determined by the presence of a low-lying LUMO, essentially consisting of the π^*_{CO} perpendicular to the acyl plane.[12c,23a] Such an empty low-lying π^*_{CO} makes the acyl carbon strongly electrophilic, thus favoring a second migration which leads to the η^2-ketone. We found that the π^*_{CO} orbital is lower in energy for the bis-methoxycalixarene complex than for the bis-cyclopentadienyl one (−10.2 *vs* −9.3 eV) so that it should undergo more easily the migration of the second alkyl group having carbanion character. This could therefore explain why, unlike for [Cp_2ZrR_2], it was impossible to isolate the [calix[4]-$(OMe)_2(O)_2$Zr(η^2-MeCO)(Me)] intermediate. Moreover, in the calculated most stable structure **F**, π^*_{CO} points toward the Me substituent, while for the [Cp_2Zr] system, π^*_{CO} is perpendicular to the plane containing the Me group.

The investigation on the migratory insertion of isocyanide into the same Zr−C bonds led us to stress the major differences both with CO and with the [Cp_2Zr]$^{2+}$ fragment. The initial stages of the isocyanide attack have been simulated as before, by performing calculations on the [calix[4]-$(OMe)_2$-$(O)_2ZrMe_2$]···CNMe system varying the carbon(*C*NMe)-to-metal distance along a line in the *xz* plane forming an angle of approximately 45° with the *z*-axis (an **A**-like approach), relaxing the R−Zr−R angle, the dihedral angle between the MeZrMe and OZrO planes and the CNMe angular position. The total energy profiles are reported in Figure 7 and show an energy barrier higher than that for the CO attack (0.4 eV instead of 0.2 eV), probably due to the higher steric hindrance of the isocyanide species.

Also in the migratory insertion of MeNC, we should invoke the intermediacy of [calix[4]-$(OMe)_2(O)_2$Zr(η^2-MeN═CMe)-(Me)], for which four hypothetical forms corresponding to those of the η^2-acyl (see Scheme 5) have been considered. In our calculations, we kept the Zr−C(methyl), Zr−C(iminoacyl), and C−N distances and the C(iminoacyl)−N−C and C−C(iminoacyl)−N angles fixed with the values taken from the X-ray structure of the bis-η^2-iminoacyl complex **15** and optimized the Zr−C−N and the C(methyl)−Zr−C(iminoacyl) angles, analogous to α and β in Scheme 5. The results have shown that the most stable structure is again that with the η^2-planar moiety lying perpendicular to the *yz* plane (**C**-like). A comparison of the orbital energies and Mulliken charges of [calix[4]-$(OMe)_2(O)_2$Zr(η^2-MeCO)(Me)] and [calix[4]-$(OMe)_2$-$(O)_2$Zr(η^2-MeN═CMe)(Me)] aids in the explanation of the different behavior of the [ZrR_2] functionality toward the migratory insertion of carbon monoxide and isocyanides. We found the π^*_{CO} orbital in the η^2-acyl species slightly lower than the π^*_{CN} orbital in the η^2-iminoacyl (−10.2 *vs* −9.9 eV, respectively) and a much higher charge on the acyl carbon than on the iminoacyl one (+0.67 *vs* +0.26 eV, respectively). The higher electrophilicity of the acyl carbon could explain the more facile migration of the second alkyl group to the η^2-acyl, leading to the η^2-ketone as the only observed product. For Bu^{t}NC, the lower electrophilicity of the iminoacyl carbon opens the possibility of observing the migratory insertion of Bu^{t}NC into the second metal−carbon bond to give the bis-η^2-iminoacyl complex, before an intramolecular migration of the alkyl group to the η^2-iminoacyl carbon takes place to give an η^2-imine species.

We finally turned our attention to the intramolecular C−C coupling of the two coordinated η^2-iminoacyl ligands in complexes **15** and **16**, leading to the formation of the enediamido complexes **17** and **18**. A complete theoretical analysis of this reaction has not been performed, due to the high number of geometrical parameters which should be simultaneously considered to take into account all of the possible degrees of freedom of the two η^2-iminoacyl groups during their coupling. However, a few qualitative conclusions can be drawn on the basis of a previous theoretical study on the intramolecular coupling of two η^2-acyl groups in organoactinide compounds [$Cp_2M(\eta^2$-$RCO)_2$] (M = Th, U). Indeed, such a study[23b] has shown that the energy of the π^*_{CO} orbitals is an important factor in determining the barrier to C−C bond coupling. A similar argument can be reasonably applied to the coupling of two η^2-iminoacyl groups. Therefore, the relatively high energy of the π^*_{CN} orbital leads to a significant barrier to the C−C coupling and makes possible the isolation of the bis-η^2-iminoacyls, at least at low temperature.

Acknowledgment. This paper is dedicated to Prof. Dieter Seebach on the occasion of his 60th birthday. We thank the Fonds National Suisse de la Recherche Scientifique (FNS, Bern, Switzerland, grant no. 20-46'590.96), CIBA-GEIGY SA (Basel, Switzerland), and Fondation Herbette (University of Lausanne, N.R.) for financial support.

Supporting Information Available: X-ray crystallography and kinetic measurements, ORTEP drawings, tables giving crystal data and details of the structure determination, atomic coordinates, anisotropic thermal parameters, bond lengths, bond angles for **5**, **13**−**15**, and **17**; table of activation parameters for **15** and **16** (44 pages). See any current page for ordering and Internet access instructions.

JA9708225

(23) (a) Tatsumi, K.; Nakamura, A.; Hoffmann, R. *Organometallics* **1985**, *4*, 404. (b) Tatsumi, K.; Nakamura, A.; Hofmann, P.; Hoffmann, R.; Moloy, K. G.; Marks, T. J. *J. Am. Chem. Soc.* **1986**, *108*, 4467.